Supporting Information: Coherent Ring-Current Dynamics of Mg-phthalocyanine probed by Time-Resolved Circular Dichroism

Shichao Sun,* Haiwang Yong, Feng Chen, and Shaul Mukamel*

Department of Chemistry and Department of Physics & Astronomy, University of California, Irvine

E-mail: shichas2@uci.edu; smukamel@uci.edu

Contents

S1 Derivation of Time-Resolved Circular Dichroism **S-2**

S2 Valence and Core Excited States **S-6**

S3 Population Dynamics **S-9**

S4 Mg K-edge TRXCD Spectrum **S-9**

S5 Peak assignment of the CD spectrum at 10.40 fs **S-10**

S6 The Induced Magnetic Field **S-11**

S7 Decomposition of Induced Magnetic Field **S-13**

S8 TRXCD Spectrum with Pure Dephasing **S-14**

S9 Calculation of Local Ring Current **S-14**

S1 Derivation of Time-Resolved Circular Dichroism

The electronic dynamics driven by the pump pulse is simulated by the evolution of wave function. Here we derive the TRCD signal induced by the probe pulse.

A Gaussian enveloped wave with amplitude Am, central frequency ω_c and duration σ, $W(t) = Am\, e^{-\frac{(t-T)^2}{2\sigma^2}}(e^{-i\omega_c t} + e^{i\omega_c t})$, can be expanded by frequency components $W(t) = \frac{1}{2\pi}\int_{-\infty}^{\infty} d\omega[e^{i\omega t}\tilde{W}_+(\omega) + e^{-i\omega t}\tilde{W}_-(\omega)]$, where

$$\tilde{W}_+(\omega) = Am \int_{-\infty}^{\infty} dt e^{-i\omega t} e^{-\frac{(t-T)^2}{2\sigma^2}} e^{i\omega_c t} = \sqrt{2\pi}\sigma\left[e^{-i(\omega-\omega_c)T} e^{-\frac{\sigma^2}{2}(\omega-\omega_c)^2}\right] \tag{S1}$$

$$\tilde{W}_-(\omega) = Am \int_{-\infty}^{\infty} dt e^{i\omega t} e^{-\frac{(t-T)^2}{2\sigma^2}} e^{-i\omega_c t} = \sqrt{2\pi}\sigma\left[e^{i(\omega-\omega_c)T} e^{-\frac{\sigma^2}{2}(\omega-\omega_c)^2}\right] \tag{S2}$$

The vector potential of Gaussian enveloped probe pulse with unit vector of polarization vector $\boldsymbol{\epsilon}$ can be written as

$$\begin{aligned}\mathbf{A}(\mathbf{r},t) &= \frac{1}{2\pi}\int_{-\infty}^{\infty} d\omega(\tilde{W}_-(\omega)\boldsymbol{\epsilon} e^{i(\mathbf{k}\cdot\mathbf{r}-\omega t)} + \tilde{W}_+(\omega)\boldsymbol{\epsilon}^* e^{-i(\mathbf{k}\cdot\mathbf{r}-\omega t)}) \\ &= \int_{-\infty}^{\infty} d\omega(\mathbf{A}^-(\omega,\mathbf{r},t) + \mathbf{A}^+(\omega,\mathbf{r},t))\end{aligned} \tag{S3}$$

where $\mathbf{A}^-(\omega,\mathbf{r},t) = \frac{1}{2\pi}\tilde{W}_-(\omega)\boldsymbol{\epsilon} e^{i(\mathbf{k}\cdot\mathbf{r}-\omega t)}$ and $\mathbf{A}^+(\omega,\mathbf{r},t) = \frac{1}{2\pi}\tilde{W}_+(\omega)\boldsymbol{\epsilon} e^{-i(\mathbf{k}\cdot\mathbf{r}-\omega t)}$.

With rotating wave approximation, the signal at photon frequency ω_1 is

$$S(\omega_1) = -\frac{2}{\hbar} Im \int d\mathbf{r} dt\ \langle \mathbf{j}^-(\mathbf{r},t)\cdot\mathbf{A}^+(\omega_1,\mathbf{r},t)\rangle \tag{S4}$$

To first order, from Fig. S1, with rotating wave approximation, we have first order ex-

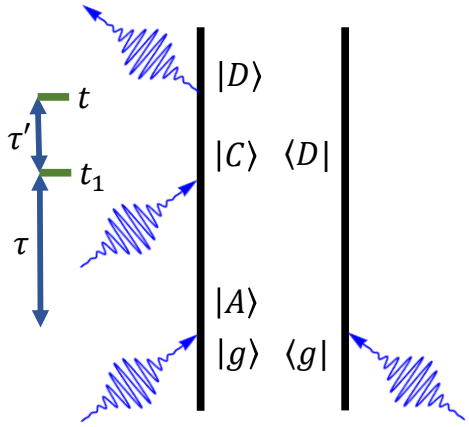

Figure S1. Ladder diagram of X-ray TRXCD. We only consider the excited state absorption contribution.

pression

$$S^{(1)}(\omega_1) = -\frac{2}{\hbar} Im \int d\mathbf{r} dt \int d\mathbf{r}_1 dt_1 d\omega_2 \left(-\frac{i}{\hbar} \langle \mathbf{j}^-(\mathbf{r},t) \cdot \mathbf{A}^+(\omega_1,\mathbf{r},t)\, \mathbf{j}^+(\mathbf{r_1},t_1) \cdot \mathbf{A}^-(\omega_2,\mathbf{r_1},t_1) \rangle \right) \tag{S5}$$

change from Heisenberg picture to Schrödinger picture,

$$S^{(1)}(\omega_1) = -\frac{2}{\hbar} Im \int d\tau d\tau' \int d\mathbf{r} d\mathbf{r}_1 \int d\omega_2 \left(-\frac{i}{\hbar} \right) \tag{S6}$$

$$\langle U^\dagger(\tau') \mathbf{j}^-(\mathbf{r}) \cdot \mathbf{A}^+(\omega_1,\mathbf{r},\tau+\tau') U(\tau) \mathbf{j}^+(\mathbf{r_1}) \cdot \mathbf{A}^-(\omega_2,\mathbf{r_1},\tau) \rangle \tag{S7}$$

expand with electronic states, the bracket expression can be expressed as

$$\begin{aligned} S^{(1)}(\omega_1) = & -\frac{2}{\hbar} Im \int d\tau d\tau' \int d\mathbf{r} d\mathbf{r}_1 \int d\omega_2 \left(-\frac{i}{\hbar} \right) \sum_{ACD} a_D^*(\tau) a_A(\tau) \langle D|U^\dagger(\tau')|D\rangle \\ & \langle D|\mathbf{j}(\mathbf{r}) \cdot \boldsymbol{\epsilon}^\dagger|C\rangle \tilde{W}_+(\omega_1) e^{i\omega_1(\tau+\tau')} e^{-i\mathbf{k}\cdot\mathbf{r}} \langle C|U(\tau')|C\rangle \langle C|\mathbf{j}^\dagger(\mathbf{r}_1) \cdot \boldsymbol{\epsilon}|A\rangle \tilde{W}_-(\omega_2) e^{-i\omega_2\tau} e^{i\mathbf{k}\cdot\mathbf{r}_1} \\ = & -\frac{2}{\hbar} Im \int d\tau d\tau' \int d\omega_2 \left(-\frac{i}{\hbar} \right) \tilde{W}_+(\omega_1) \tilde{W}_-(\omega_2) \\ & \times \sum_{ACD} a_D^*(\tau) a_A(\tau) \mathbf{j}_{DC}(\mathbf{k}) \cdot \boldsymbol{\epsilon}^\dagger\, \mathbf{j}_{CA}^\dagger(-\mathbf{k}) \cdot \boldsymbol{\epsilon} e^{i(E_D - E_C + \omega_1)\tau'} e^{-i(\omega_2-\omega_1)\tau} \end{aligned} \tag{S8}$$

where $\mathbf{k} = \frac{\omega_1}{c}\hat{\mathbf{e}}_k$. Multiplying by damping factor to account for core states (index C) decay, and integrate τ, τ',

$$S^{(1)}(\omega_1) = -\frac{2}{\hbar} Im\left(-\frac{i}{\hbar}\right) \sum_{ACD} \mathbf{j}_{DC}(\mathbf{k}) \cdot \boldsymbol{\epsilon}^\dagger \mathbf{j}^\dagger_{CA}(-\mathbf{k}) \cdot \boldsymbol{\epsilon} \int d\omega_2 \int_0^{+\infty} d\tau \int_0^{+\infty} d\tau' \\ \tilde{W}_+(\omega_1)\tilde{W}_-(\omega_2) a^*_D(\tau) a_A(\tau) e^{-i(\omega_2-\omega_1)\tau} e^{i(E_D - E_C + \omega_1)\tau'} e^{-\Gamma\tau'} \tag{S9}$$

To account for dephasing of the excited state coherences, we multiply pure dephasing factor $\exp[-\Gamma_{1,DA}\tau]$ for the coherence of excited state $A - D$, and factor $\exp[-\Gamma_{2,DC}\tau']$ for the valence-core state dephasing,

$$\begin{aligned} S^{(1)}(\omega_1) =& \frac{2}{\hbar^2} Im\, i \sum_{ACD} \mathbf{j}_{DC}(\mathbf{k}) \cdot \boldsymbol{\epsilon}^\dagger \mathbf{j}^\dagger_{CA}(-\mathbf{k}) \cdot \boldsymbol{\epsilon} \int_0^{+\infty} d\tau \int_0^{+\infty} d\tau'\, Am \\ & \tilde{W}_+(\omega_1) e^{-\frac{\tau^2 + T^2 - 2\tau(T + i\sigma^2(\omega_1 - \omega_c))}{2\sigma^2}} a^*_D(\tau) a_A(\tau) e^{-\Gamma_{1,DA}\tau} e^{i(E_D - E_C + \omega_1)\tau'} e^{-(\Gamma + \Gamma_{2,DC})\tau'} \\ =& \frac{2}{\hbar^2} Im\, i \sum_{ACD} \mathbf{j}_{DC}(\mathbf{k}) \cdot \boldsymbol{\epsilon}^\dagger \mathbf{j}^\dagger_{CA}(-\mathbf{k}) \cdot \boldsymbol{\epsilon} \frac{i}{E_D - E_C + \omega_1 + i(\Gamma + \Gamma_{2,DC})} \int_0^{+\infty} d\tau\, Am \\ & \tilde{W}_+(\omega_1) e^{-\frac{\tau^2 + T^2 - 2\tau(T + i\sigma^2(\omega_1 - \omega_c))}{2\sigma^2}} e^{-\Gamma_{1,DA}\tau} a^*_D(\tau) a_A(\tau) \\ =& -\frac{2}{\hbar^2} Im \Bigg\{ \sum_{ACD} \frac{\mathbf{j}_{DC}(\mathbf{k}) \cdot \boldsymbol{\epsilon}^\dagger \mathbf{j}^\dagger_{CA}(-\mathbf{k}) \cdot \boldsymbol{\epsilon}}{E_D - E_C + \omega_1 + i(\Gamma + \Gamma_{2,DC})} \int_0^{+\infty} d\tau\, Am \\ & \tilde{W}_+(\omega_1) e^{-\frac{\tau^2 + T^2 - 2\tau(T + i\sigma^2(\omega_1 - \omega_c))}{2\sigma^2}} e^{-\Gamma_{1,DA}\tau} a^*_D(\tau) a_A(\tau) \Bigg\} \end{aligned} \tag{S10}$$

where E_A and E_D are the energy of ground state and valence excited states, E_C is the energy of core excited states. The integral of τ is a numerical integration since $a^*_D(\tau)a_A(\tau)$ is given by the electronic dynamics.

The circular dichroism is defined as the difference of absorption of left and right circularly polarized light, $S_{CD} = S_- - S_+$. Define the polarization unit vector of circularly polarized wave as $\boldsymbol{\epsilon}_\pm(\gamma) = \frac{1}{\sqrt{2}}(\boldsymbol{\epsilon}_\alpha \pm i\boldsymbol{\epsilon}_\beta)$, where γ is the propagation direction of the wave, α, β and γ are perpendicular to each other and follow right hand rule. Specially, a wave propagating in z direction has circular polarization $\boldsymbol{\epsilon}_\pm(z) = \frac{1}{\sqrt{2}}(\boldsymbol{\epsilon}_x \pm i\boldsymbol{\epsilon}_y)$. Here the unit vector of propagation

direction vector is $\boldsymbol{\epsilon}_\kappa$, we have relation

$$\mathbf{p}\cdot\boldsymbol{\epsilon}_-^\dagger\,\mathbf{q}\cdot\boldsymbol{\epsilon}_- - \mathbf{p}\cdot\boldsymbol{\epsilon}_+^\dagger\,\mathbf{q}\cdot\boldsymbol{\epsilon}_+ = -i\mathbf{p}\times\mathbf{q}\cdot\boldsymbol{\epsilon}_\kappa$$

where $\mathbf{p}$ and $\mathbf{q}$ are arbitrary vectors.

The CD signal can be written as

$$\begin{aligned}
S_{\mathrm{CD}}(\omega_1) =& -\frac{2}{\hbar^2}Im\Bigg\{\sum_{ACD}\frac{-i\,\mathbf{j}_{DC}(\mathbf{k})\times\mathbf{j}_{CA}^\dagger(-\mathbf{k})}{E_D-E_C+\omega_1+i(\Gamma+\Gamma_{2,DC})}\cdot\boldsymbol{\epsilon}_\kappa\, Am \\
&\int_0^{+\infty}d\tau\tilde{W}_+(\omega_1)e^{-\frac{\tau^2+T^2-2\tau(T+i\sigma^2(\omega_1-\omega_c))}{2\sigma^2}}e^{-\Gamma_{1,DA}\tau}a_D^*(\tau)a_A(\tau)\Bigg\} \\
=&\frac{2}{\hbar^2}Re\Bigg\{\tilde{W}_+(\omega_1)\sum_{ACD}\frac{\mathbf{j}_{DC}(\mathbf{k})\times\mathbf{j}_{CA}^\dagger(-\mathbf{k})}{E_D-E_C+\omega_1+i(\Gamma+\Gamma_{2,DC})}\cdot\boldsymbol{\epsilon}_\kappa\, Am \\
&\int_0^{+\infty}d\tau\, e^{-\frac{\tau^2+T^2-2\tau(T+i\sigma^2(\omega_1-\omega_c))}{2\sigma^2}}e^{-\Gamma_{1,DA}\tau}a_D^*(\tau)a_A(\tau)\Bigg\} \\
=&\frac{2}{\hbar^2}Re\Bigg\{\tilde{W}_+(\omega_1)\sum_{ACD}\frac{\mathbf{j}_{DC}(\mathbf{k})\times\mathbf{j}_{CA}^\dagger(-\mathbf{k})}{E_D-E_C+\omega_1+i(\Gamma+\Gamma_{2,DC})}\cdot\boldsymbol{\epsilon}_\kappa\, Am \\
&\int_0^{+\infty}d\tau\, e^{-\frac{(\tau-T)^2}{2\sigma^2}}e^{i\tau(\omega_1-\omega_c)}e^{-\Gamma_{1,DA}\tau}a_D^*(\tau)a_A(\tau)\Bigg\}
\end{aligned}\tag{S11}$$

To avoid numerical instability, insert the definition of $\tilde{W}_+(\omega_1)$ and simplify, we have

$$\begin{aligned}
S_{\mathrm{CD}}(\omega_1) =& \frac{2(Am)^2}{\hbar^2}Re\Bigg\{\sqrt{2\pi}\sigma e^{-i(\omega_1-\omega_c)T}e^{-\frac{\sigma^2(\omega_1-\omega_c)^2}{2}} \\
&\sum_{ACD}\frac{\mathbf{j}_{DC}(\mathbf{k})\times\mathbf{j}_{CA}^\dagger(-\mathbf{k})}{E_D-E_C+\omega_1+i(\Gamma+\Gamma_{2,DC})}\cdot\boldsymbol{\epsilon}_\kappa\int_0^{+\infty}d\tau\, e^{-\frac{(\tau-T)^2}{2\sigma^2}}e^{i\tau(\omega_1-\omega_c)}e^{-\Gamma_{1,DA}\tau}a_D^*(\tau)a_A(\tau)\Bigg\} \\
=& \frac{2(Am)^2}{\hbar^2}\sqrt{2\pi}\sigma Re\Bigg\{\sum_{ACD}\frac{\mathbf{j}_{DC}(\mathbf{k})\times\mathbf{j}_{CA}^\dagger(-\mathbf{k})}{E_D-E_C+\omega_1+i(\Gamma+\Gamma_{2,DC})}\cdot\boldsymbol{\epsilon}_\kappa \\
&\int_0^{+\infty}d\tau\, e^{i(\omega_1-\omega_c)(\tau-T)}e^{-\frac{1}{2}\left[\frac{(\tau-T)^2}{\sigma^2}+\sigma^2(\omega_1-\omega_c)^2\right]}e^{-\Gamma_{1,DA}\tau}a_D^*(\tau)a_A(\tau)\Bigg\}
\end{aligned}\tag{S12}$$

In this work, the probe wave propagate in z direction. Take zero dephasing approximation,

where $\Gamma_{2,DC} = 0$ and $\Gamma_{1,DA} = 0$, and normalize by $(Am)^2$, Eq. (S12) become Eq. (3). In section S8 we will compare the effects of different dephasing factors.

S2 Valence and Core Excited States

Table S1. Excited states of Mg-phthalocyanine with nonzero oscillator strength. The transition electric dipoles $\langle g|\boldsymbol{\mu}|e\rangle$ are in atomic unit ea_0.

state	energy (eV)	$\langle g\|\mu_x\|e\rangle$	$\langle g\|\mu_y\|e\rangle$	$\langle g\|\mu_z\|e\rangle$
$1E_u$x	2.26596903	3.2204	0.0000	0.0000
$1E_u$y	2.26596903	0.0000	-3.2204	0.0000
$2E_u$x	3.36094484	-0.4366	0.0000	0.0000
$2E_u$y	3.36094484	0.0000	0.4366	0.0000
$3E_u$x	3.65324515	0.7392	0.0000	0.0000
$3E_u$y	3.65324515	0.0000	0.7392	0.0000
$4E_u$x	3.75545851	1.6162	0.0000	0.0000
$4E_u$y	3.75545851	0.0000	1.6162	0.0000
A_{2u}	3.88113308	0.0000	0.0000	0.2339
$5E_u$x	3.95713036	1.0779	0.0000	0.0000
$5E_u$y	3.95713036	0.0000	1.0779	0.0000
$6E_u$x	4.00836971	-3.1249	0.0000	0.0000
$6E_u$y	4.00836971	0.0000	3.1249	0.0000
$7E_u$x	4.49228381	3.3076	0.0000	0.0000
$7E_u$y	4.49228381	0.0000	-3.3076	0.0000

Table S2. Nitrogen K-edge core excited states of Mg-phthalocyanine. Only spin singlet states are listed.

state	irreducible representation	energy (eV)
1		386.1709
2	E_g	386.1711
3	E_g	386.1711
4		386.1713
5		386.2963
6	E_g	386.2966
7	E_g	386.2966
8		386.2972

9		386.3726
10		386.3726
11	E_g	386.3726
12	E_g	386.3726
13		386.4589
14		386.4589
15	E_g	386.4590
16	E_g	386.4590
17	B_{1u}	388.1611
18	E_g	388.1612
19	E_g	388.1612
20	A_{2u}	388.1615
21	B_{2u}	388.2934
22	E_g	388.2939
23	E_g	388.2939
24	A_{2u}	388.2946
25	B_{1u}	388.3277
26	E_g	388.3280
27	E_g	388.3280
28	A_{1u}	388.3284
29	B_{2u}	388.6100
30	E_g	388.6101
31	E_g	388.6101
32	A_{1u}	388.6103
33	A_{2u}	388.7521
34	E_g	388.7521
35	E_g	388.7521
36	B_{1u}	388.7522
37	A_{2u}	388.8027
38	E_g	388.8028
39	E_g	388.8028
40	B_{2u}	388.8029
41		389.0340
42		389.0340
43	E_g	389.0340
44	E_g	389.0340
45		389.0719
46	E_g	389.0720
47	E_g	389.0720

48		389.0720
49		389.1107
50		389.1108
51	E_g	389.1108
52	E_g	389.1108
53	A_{2u}	389.1601
54	E_g	389.1602
55	E_g	389.1602
56	B_{1u}	389.1602
57	A_{1g}	389.6734
58	E_u	389.6735
59	E_u	389.6735
60	B_{1g}	389.6738
61	A_{1g}	389.9651
62	E_u	389.9652
63	E_u	389.9652
64	B_{2g}	389.9655
65	A_{2u}	389.9825
66	E_g	389.9827
67	E_g	389.9827
68	B_{2u}	389.9830
69	A_{1u}	390.0015
70	E_g	390.0015
71	E_g	390.0015
72	B_{2u}	390.0016
73	A_{1u}	390.0205
74	E_g	390.0206
75	E_g	390.0206
76	B_{1u}	390.0208
77		390.2204
78	E_g	390.2205
79	E_g	390.2205
80		390.2208

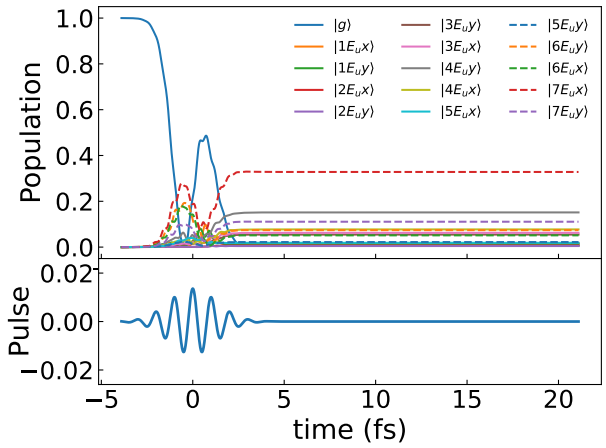

Figure S2. Population dynamics in the upper panel, pulse in the lower panel.

S3 Population Dynamics

The valence excited state population contributes to the population ring currents. After the pulse is over, the population is a constant.

S4 Mg K-edge TRXCD Spectrum

The TRXCD spectrum of Mg K-edge is displayed in Fig. S3. Due to the large core state line width of 0.45 eV, different core excited states cannot be resolved in the spectrum. We thus do not use Mg K-edge for analysis.

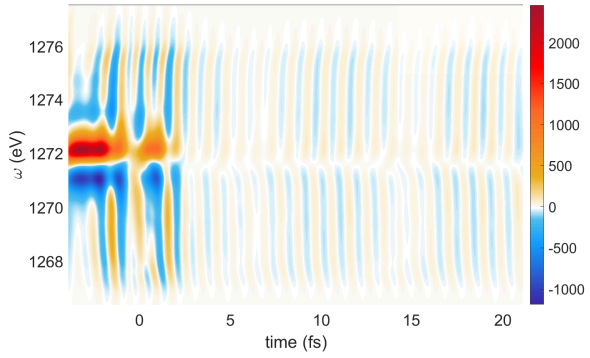

Figure S3. Time-resolved circular dichroism (Eq. 3) of Mg K-edge.

S5 Peak assignment of the CD spectrum at 10.40 fs

The Nitrogen K-edge X-ray CD spectrum at 10.40 fs is shown in Fig. S4. We assign the peaks by evaluating $\frac{\mathbf{j}_{DC}(\mathbf{k})\times\mathbf{j}^{\dagger}_{CA}(-\mathbf{k})}{E_D-E_C+\omega+i\Gamma}$ in Eq. (3).

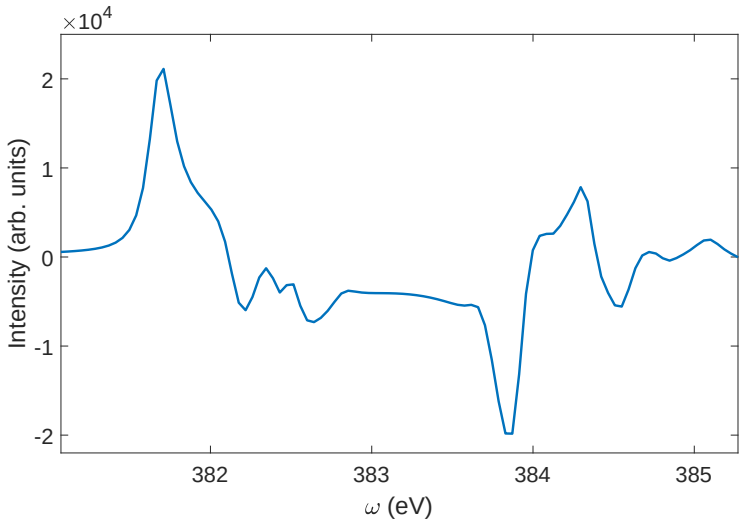

Figure S4. Nitrogen K-edge CD spectrum at 10.40 fs.

The $7E_u - 4E_u$ coherence causes 5 peaks. The peaks at 383.6690 eV and 384.4058 eV correspond to excitation to the degenerate core state 22, 23 from $7E_u$ and $4E_u$ valence state respectively. The peaks at 383.8017 eV and 384.5385 eV correspond to excitation to core state 25 from states $7E_u$ and $4E_u$ respectively. The 382.4157 eV peak represents the excitation from $4E_u$ to core states 6, 7.

The peaks at 381.6788 eV and 383.6690 eV have contributions from the excitation from $7E_u$ to degenerate core state 6, 7 and to degenerate core state 22, 23 respectively. Since they come from the $7E_u$ population, they are time-independent after the pump pulse.

The $7E_u - 6E_u$ coherence contributes to two frequencies. The peak at 381.6788 eV represents the excitation from $7E_u$ to degenerate core state 6, 7. 382.1627 eV correspond to excitation from $6E_u$ to degenerate core state 6, 7. Thus, the 382.1627 eV peak is the unique characteristic of the $7E_u - 6E_u$ coherence.

The coherence $7E_u - 1E_u$ contributes to two frequencies. Peak at 381.6788 eV excitation

from $7E_u$ to core state 6, 7. at 383.9051 eV is excitation from $1E_u$ to core state 6, 7. So, the 383.9051 is the characteristic peak of this coherence.

The coherence $7E_u - 5E_u$ corresponds to 4 peaks. 383.8017 eV is excitation from $7E_u$ to core state 25. 384.3369 eV is from $5E_u$ to core state 25. 383.6690 eV is from $7E_u$ to core state 22. 384.2041 eV is from $5E_u$ to core state 22. Thus 384.3369 and 384.2041 eV are the characteristic peaks of this coherence.

The $7E_u - 3E_u$ coherence has two peaks. 381.6788 eV is the excitation from $7E_u$ to core state 6, 7. 382.5179 eV is excitation from $3E_u$ to core state 6, 7. Thus, 382.5179 eV is the characteristic peak.

The $6E_u - 1E_u$ coherence has two peaks. 382.1627 eV, is the excitation from $6E_u$ to core state 6, 7. 383.9051 eV is from $1E_u$ to core state 6, 7. They share the same energy range as other coherence.

The $4E_u - 1E_u$ coherence has two peaks. 382.4157 eV is excitation from $4E_u$ to core state 6, 7. 383.9051 eV is excitation from $1E_u$ to core state 6, 7.

The $4E_u - 3E_u$ coherence has two peaks. 382.4157 eV is from $4E_u$ to core state 6, 7. 382.5179 eV is from $3E_u$ to core state 6, 7.

Coherence $5E_u - 1E_u$ has two peaks. 382.2140 eV is $5E_u$ to core state 6, 7. 383.9051 eV is from $1E_u$ to core state 6, 7. So 382.2140 eV is characteristic.

The peak assignment to specific coherences, the oscillation periods and the coherence frequencies are summarized in Table 2 in the main text.

S6 The Induced Magnetic Field

The induced magnetic field created by ring current can indicate the direction and strength of ring current. We use Biot-Savart law to caclculate the induced magnetic field at the center of the molecule (on Mg atom) as a function of time. Assume the molecule is in the plane of paper, z direction is pointing out of the paper to the reader, a counter-clockwise current

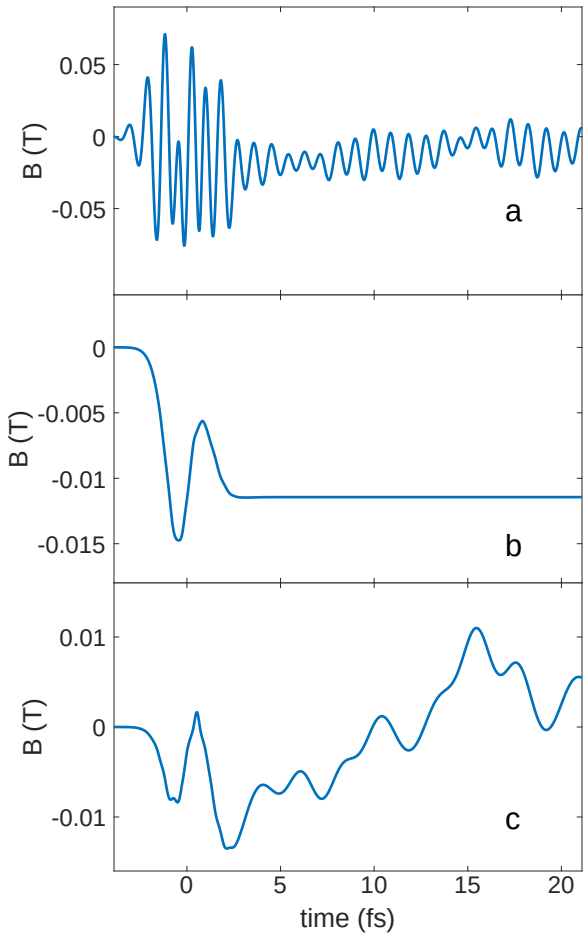

Figure S5. Time-resolved induced magnetic field. Panel a is the total induced magnetic field. Panel b is the contribution from the population ring current. After the pump pulse finish, their contribution becomes constant at -0.01144 T. Panel c is the contribution from the coherent ring current from the coherence between excited states.

will create induced magnetic field pointing into the paper, which is negative valued while the clockwise current create positive valued induced magnetic field pointing out of the paper.

The time evolution of induced magnetic field by ring current is displayed in Fig. S5. The total induced magnetic field include the contribution from population ring current, g-ex coherent current and ex-ex coherence between states with different energy. The fast oscillation in panel a is contributed by g-ex coherence due to their relatively large energy separation. The contribution from the population ring current is displayed in panel b. After the pulse, their contribution become a constant at -0.01144 T. The contribution from the

ex-ex coherent ring current is displayed in panel c.

S7 Decomposition of Induced Magnetic Field

We decompose the ex-ex coherent ring current into individual coherence pair in Fig. S6.

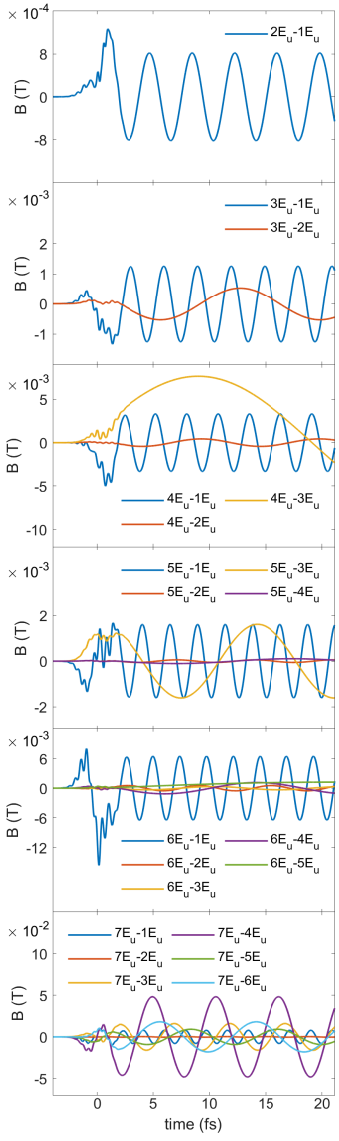

Figure S6. Contribution of the excited states coherence to the induced magnetic field.

S8 TRXCD Spectrum with Pure Dephasing

In Eq. (S12), the effect of dephasing is added as pure dephasing to describe the decoherence induced by the interaction between the molecular system with bath. The factor $e^{-\Gamma_{1,DA}\tau}$ gives rise to the decoherence of valence-valence state coherence, where index D, A run over ground and valence excited states. As will be shown in the result, the ground state-valence excited state coherence does not contribute to any change, since the coherence between ground state and valence state has a shorter oscillation period than the pulse duration, thus not observable in the time-resolved spectra. The parameter $\Gamma_{2,DC}$ give rise to the decoherence of valence-core state coherence. TRXCD spectra and their Fourier transformed spectra with different pure dephasing strength are displayed in Fig. S7. For $\Gamma_{1,DA}$ and $\Gamma_{2,DC}$ equal to $1/100$ fs^{-1}, the results are similar to no dephasing results. As the dephasing parameter increase, the TRXCD signal decay with time. Larger dephasing corresponds to earlier decay. As a result, in Fourier transformed spectra, as the dephasing parameters increase, the strength of the peaks decrease, so does the peak resolution in frequency axis ($\hbar\omega'$). Aside from that, as in Eq. (S12), $\Gamma_{2,DC}$ in the denominator will broaden the peak in energy domain. Since the value of dephasing parameter is smaller than the life time decay Γ of core excited states, this broadening is not significant.

S9 Calculation of Local Ring Current

Local ring currents are calculated by numerically integrating the current density at a plane, $I = \int_A dS\, \hat{\mathbf{n}} \cdot \mathbf{j}$, where $\mathbf{j}$ is the current density, A is the plane, $\hat{\mathbf{n}}$ is the normal vector of the plane. As depicted in Fig. S8, different plane and normal vectors are chosen for different zones. Mg atom is at the origin, with x and y axis shown in Fig. S8.

For ring α, the plane is chosen as half plane in xz plane, with boundary going through the center of benzene ring α and perpendicular to xy plane. The normal vector is the unit vector in $-y$ direction. The integration of current density in this plane gives the current

going in $-y$ direction through this plane, i.e., the current I of ring α, see top panel of Fig. 4. Similarly, the integration plane of ring γ is the half plane in xz plane, with its boundary going through the center of benzene ring γ, with normal vecor in $+y$. Positively valued $I(\alpha)$, $I(\gamma)$ indicates clockwise ring currents in ring α, γ.

The integration plane for ring β and δ are half plane in yz plane, with their boundary going through the center of benzene ring β and δ respectively. The normal vectors of β is in $-x$ direction while the normal vector for δ is in $+x$. Positively valued $I(\beta)$ and $I(\delta)$ indicates clockwise ring currents in ring β and δ respectively.

The integration plane for ring current around Mg atom (CT) is in xz plane between the Mg nucleus and the middle point of Mg and N, as the black line in Fig. S8. The normal vector is in $-y$. Positive I(CT) indicates clockwise CT ring current. Similar to CT, the integration plane for outer ring (OT) current is in xz plane between x = 3.4 Å and the middle point of Mg and N (the orange line in Fig. S8). The normal vector is in $-y$. Positive I(OT) indicates clockwise OT ring current.

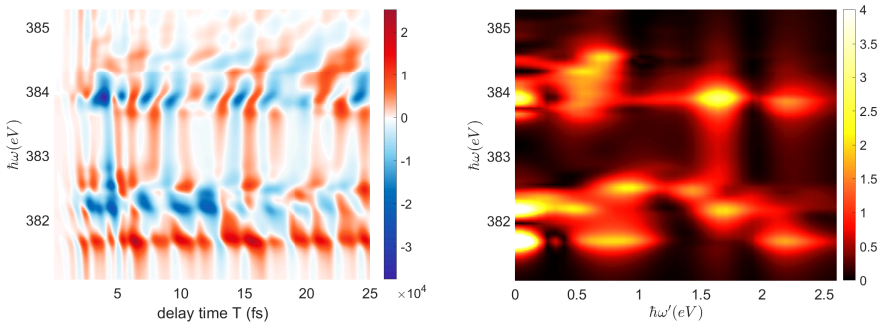

Figure S7.1. Dephasing parameters $\Gamma_{1,DA}$ and $\Gamma_{2,DC}$ both set to $1/100$ fs^{-1}.

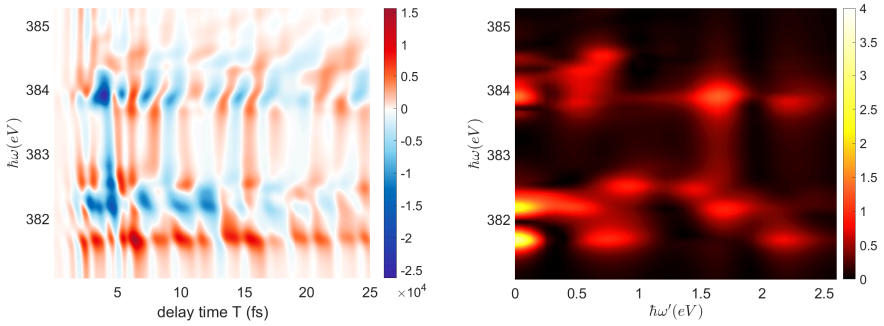

Figure S7.2. Dephasing parameters $\Gamma_{1,DA}$ and $\Gamma_{2,DC}$ both set to $1/20$ fs^{-1}.

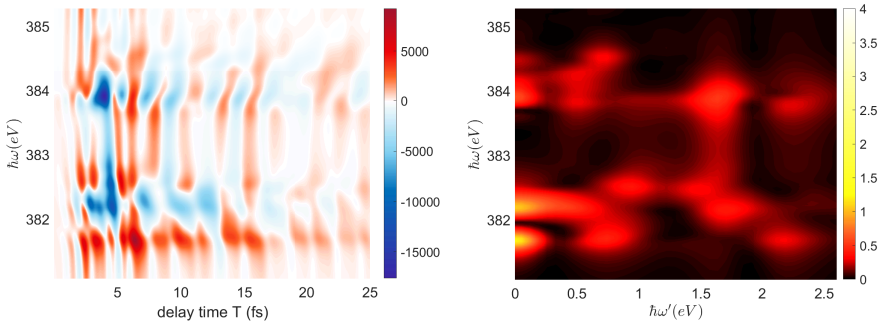

Figure S7.3. Dephasing parameters $\Gamma_{1,DA}$ and $\Gamma_{2,DC}$ both set to $1/10$ fs^{-1}.

Figure S7. Dephasing parameters $\Gamma_{1,DA}$ and $\Gamma_{2,DC}$ both set to $1/100$ fs^{-1}, $1/20$ fs^{-1} and $1/10$ fs^{-1} respectively. Left panels are TRXCD spectra, right panels are the Fourier transformed spectra. Arbitrary units are used with the same scale.

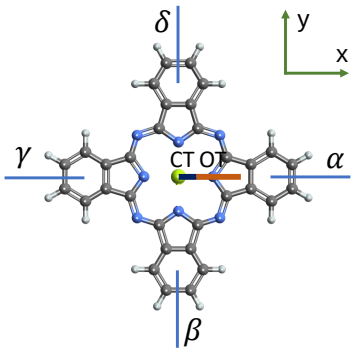

Figure S8. The integration planes for calculating the local ring currents in different zones of the molecule.